Eliassen-Palm Diagnostics of Wave–Mean Flow Interaction in the GFDL "SKYHI" General Circulation Model

D. G. ANDREWS[1]

Geophysical Fluid Dynamics Program, Princeton University, Princeton, NJ 08540

J. D. MAHLMAN AND R. W. SINCLAIR[2]

Geophysical Fluid Dynamics Laboratory/NOAA, Princeton University, Princeton, NJ 08540

(Manuscript received 11 April 1983, in final form 25 July 1983)

ABSTRACT

The Eliassen-Palm flux is important in analytical studies of small-amplitude waves where it provides a powerful and elegant tool for the description of wave propagation in mean zonal shear flows, as well as for analysis of the effective mean zonal force induced by the waves. Furthermore, it has recently been used as a diagnostic in a number of studies of atmospheric data and numerical models of specific dynamical phenomena. In this paper, we apply it to the GFDL "SKYHI" global general circulation model of the troposphere–stratosphere–mesosphere, and describe computations of the primitive equations, isobaric coordinate form of the Eliassen-Palm flux and its divergence under conditions of annual-mean insolation.

The Eliassen-Palm flux diagnostics show a clear picture of planetary wave propagation from the midlatitude troposphere into the stratosphere and mesosphere. In the tropics, the presence of Kelvin waves confuses the picture somewhat (because their phase speeds are eastward with respect to the mean flow) and necessitates additional analysis, which is given elsewhere.

We find the Eliassen-Palm diagnostics lead to new insights on the forcing of mean flows by the eddies. The implications of the fact that the model waves are not close to "non-acceleration conditions" and the importance of mean diabatic effects in our 30-day average statistics are considered in Appendix B. An important finding is that zonal westerly flows are strongly *decelerated* by eddies in the midlatitude upper troposphere and the mesosphere, in sharp contrast to the apparent implication of traditional zonal mean balances.

On the other hand, the forcing of mean accelerations by waves in the tropics is essentially in agreement with that found in earlier studies. The above inferences from the Eliassen-Palm diagnostics concerning the effect of eddies on zonal flows have been tested in a companion model experiment in which eddies propagating out of the troposphere are strongly damped. This experiment shows the resultant zonal flow accelerations to be fully consistent with the inferences from the Eliassen-Palm diagnostics.

1. Introduction

Theoretical studies of the interaction of waves with zonally-averaged flows usually split the phenomenon into two complementary parts: first, the influence of the mean-flow configuration on the propagation of the waves, and second, the nonlinear back-effect of the waves on the mean flow. Morever, recent work has shown that a vector quantity known as the *Eliassen-Palm flux* $\mathbf{F}$ (to be defined in Section 2) plays a central role in both these aspects of wave, mean-flow interaction, at least when wave amplitudes are small. On the one hand, it appears as the flux in a "conservation law" for wave properties that is simpler, and in some ways more fundamental, than the wave-energy equation (which is not generally of conservation-law type). On the other hand, its divergence represents an important forcing of the mean flow by the waves in a transformed version of the Eulerian-mean equations. (This also holds at finite amplitude.) Indeed, in the quasi-geostrophic case, it is the only such forcing term.

In several recent papers the first attempts have been made to use $\mathbf{F}$ and its divergence as diagnostics for the interpretation of wave, mean-flow interaction in observational data and numerical simulations of the atmosphere. These include, e.g., the works by Sato (1980) and Hamilton (1982) [observations of stationary planetary waves]; Edmon *et al.* (1980) [tropospheric observations and simulations of nonlinear baroclinic waves]; Hsu (1981) and Dunkerton *et al.* (1981) [simulation of a stratospheric sudden warming]; Palmer (1981) and O'Neill and Youngblut (1982) [observations of a sudden warming]; and McIntyre (1982) [theories of sudden warmings].

In the present paper we describe the computation of the Eliassen-Palm flux and its divergence as diag-

[1] Current affiliation: Department of Atmospheric Physics, Clarendon Laboratory, Parks Road, Oxford, UK.

[2] Current affiliation: Harris Systems, Inc., Melbourne, FL 32901.

nostics in the GFDL "SKYHI" general circulation model (GCM) of the troposphere, stratosphere and mesosphere. This is a global finite-difference model with 40 levels in the vertical, with the highest level near 80 km. Some further details of the model are given in Fels *et al.* (1980; hereafter designated FMSS) and in Section 4 of this paper.

The work reported here is exploratory in nature and is intended to start the investigation of two separate issues. First, we wish to discover whether the model can help us to assess the advantages and shortcomings of the Eliassen-Palm diagnostics as tools for dynamical interpretation of the middle atmosphere. Second, the diagnostics point to model strengths and weaknesses in simulating wave behavior in the middle atmosphere. At present, we have restricted attention to the routine use of the Eliassen-Palm diagnostics in extended model runs over long time periods. Future studies will concentrate on more specific dynamical events, particularly in seasonal integrations with this GCM.

2. Theoretical background

The Eliassen-Palm (E-P) flux can be written in pressure coordinates on the sphere as

$$\mathbf{F} = \{F_{(\phi)}, F_{(p)}\} = a\cos\phi\left\{-\overline{u'v'} + \psi\frac{\partial\bar{u}}{\partial p}, -\overline{u'\omega'} - \psi\left[\frac{\partial(\bar{u}\cos\phi)}{a\cos\phi\partial\phi} - f\right]\right\}, \quad (2.1)$$

where

$$\psi = \overline{v'\theta'}\Big/\frac{\partial\bar{\theta}}{\partial p} = -\overline{v'T'}\Big/\left(\frac{\kappa\bar{T}}{p} - \frac{\partial\bar{T}}{\partial p}\right). \quad (2.2)$$

[See, e.g., Eliassen-Palm (1961); Andrews and McIntyre (1976, 1978a); Boyd (1976).] Here ϕ represents latitude, p pressure, (u, v, ω) the "velocity" in (longitude, latitude, pressure) coordinates, θ the potential temperature, T the temperature, a the earth's radius, f the Coriolis parameter and κ the ratio of the gas constant to the specific heat at constant pressure. Overbars denote zonal "Eulerian" averages at constant ϕ and p and primes denote departures therefrom.

We define the isobaric "divergence" of $\mathbf{F}$ by

$$\nabla\cdot\mathbf{F} = \frac{\partial(F_{(\phi)}\cos\phi)}{a\cos\phi\partial\phi} + \frac{\partial F_{(p)}}{\partial p}. \quad (2.3)$$

It has been shown by Andrews and McIntyre (1976, 1978a) that a "generalized Eliassen-Palm theorem" of the following form holds for small-amplitude disturbances (waves) on a basic zonal flow:

$$\frac{\partial A}{\partial t} + \nabla\cdot\mathbf{F} = D + O(\text{amplitude})^3. \quad (2.4)$$

In this equation $\partial A/\partial t$ represents wave transience and D involves nonconservative effects (such as dissipation or forcing) in the waves. These terms, like $\mathbf{F}$, are of second order in wave amplitude; explicit expressions for A and D are given by Andrews and McIntyre (1978a). A quasi-geostrophic approximation to A has been given by Edmon *et al.* (1980), who have called A "the density of E-P wave activity." The $O(\text{amplitude})^3$ term represents nonlinear effects and vanishes for purely linear waves. It is important to note that A and D generally involve fluid particle displacements [e.g., Andrews and McIntyre, 1978a, Eq. (3.12a)], and so cannot be calculated unambiguously from observational data and most numerical models, including ours. Moreover, their signs depend on the waves under consideration. For example, Edmon *et al.* (1980) showed that A is positive for quasi-geostrophic disturbances on a positive potential vorticity gradient; but for equatorial Kelvin waves, and other waves with eastward phase speed relative to the mean flow, A is negative (C.-P. F. Hsu, private communication, 1980; Edmon *et al.* (1980).

Equation (2.4) is of "conservation law" form when the right-hand side is zero, that is, for linear conservative waves. To this extent it is analogous to the "wave-action equation" (cf Bretherton and Garrett, 1968; Andrews and McIntyre, 1978b; McIntyre, 1980), but of simpler form than the "wave-energy equation", which generally involves further terms representing exchange of energy between the waves and the mean flow.

A second place where $\mathbf{F}$ appears is in a transformed version of the mean-flow equations. The familiar "Eulerian-mean" form of the zonally-averaged zonal momentum equation is

$$\frac{\partial\bar{u}}{\partial t} = \left[-\left(\frac{\partial(\bar{u}\cos\phi)}{a\cos\phi\partial\phi} - f\right)\bar{v} - \frac{\partial\bar{u}}{\partial p}\bar{\omega}\right] + \left\{-\frac{\partial(\overline{u'v'}\cos^2\phi)}{a\cos^2\phi\partial\phi} - \frac{\partial(\overline{u'\omega'})}{\partial p}\right\} + \bar{X}, \quad (2.5)$$

where $\bar{X}$ is any mean nonconservative force such as diffusion. However, if we introduce the "residual" mean meridional circulation

$$\bar{v}^* \equiv \bar{v} - \frac{\partial\psi}{\partial p}, \quad \bar{\omega}^* \equiv \bar{\omega} + \frac{\partial(\psi\cos\phi)}{a\cos\phi\partial\phi}, \quad (2.6)$$

we obtain the transformed mean zonal momentum equation (e.g. Andrews and McIntyre 1978a)

$$\frac{\partial\bar{u}}{\partial t} = \left[-\left(\frac{\partial(\bar{u}\cos\phi)}{a\cos\phi\partial\phi} - f\right)\bar{v}^* - \frac{\partial\bar{u}}{\partial p}\bar{\omega}^*\right] + \left\{\frac{1}{a\cos\phi}\nabla\cdot\mathbf{F}\right\} + \bar{X}. \quad (2.7)$$

In contrast to (2.5), this incorporates $(\bar{v}^*, \bar{\omega}^*)$ instead of $(\bar{v}, \bar{\omega})$ in the mean meridional advection term (in

the brackets) and $\nabla \cdot \mathbf{F}$ in place of the Reynolds stress divergence term (in the braces). Unlike $\mathbf{F}$, the Reynolds stress does not appear as the flux in a conservation law for wave properties. A complete set of mean-flow equations in the transformed formalism is given, for example, by Dunkerton *et al.* (1981).

The philosophy underlying the use of $\mathbf{F}$ and $\nabla \cdot \mathbf{F}$ as diagnostics of wave, mean-flow interaction is explained in detail by Edmon *et al.* (1980) and McIntyre (1982), and will only be briefly summarized here. First, the conservation law (2.4) suggests that $\mathbf{F}$ can be regarded as a "flux of wave-activity" which is dynamically less ambiguous than the "flux of wave-energy". Second, the appearance of $\nabla \cdot \mathbf{F}$ in (2.7) makes it an important part of the forcing of the mean flow by the waves. Its significance is further enhanced by the fact that, under quasi-geostrophic scaling, the wave-induced forcing in the transformed thermodynamic equation becomes negligible, leaving $\nabla \cdot \mathbf{F}$ as the only wave forcing in the transformed mean equations of motion [Edmon *et al.*, 1980, Eq. (3.3); and Appendix B]. (A simple result like this does not hold for the untransformed quasi-geostrophic equations.)

3. Model E-P flux diagnostics

Our basic aim is similar to that of the papers mentioned in Section 1, namely to calculate from the model output and plot in the meridional plane, arrows representing the E-P flux vector $\mathbf{F}$ and contours of its divergence. We shall also present the latitudinal variation of the separate terms in the two forms (2.5) and (2.7) of the time mean, zonally averaged momentum equation at various heights.

Since we are considering a large depth of atmosphere (about 12 pressure scale-heights) it is clearly more convenient to use $z \equiv -\ln(p/1013 \text{ mb})$ than pressure p as the vertical coordinate in meridional cross sections. It is therefore necessary to transform the pressure-coordinate version (2.1) of $\mathbf{F}$ to the log-pressure coordinate form $\tilde{\mathbf{F}}$. (Some details are presented in Appendix A, together with information on the computation of the diagnostics.)

A difficulty which now emerges is that $|\tilde{\mathbf{F}}|$ decays rapidly with height, owing to wave dissipation. Thus, some further rescaling of the $\tilde{\mathbf{F}}$-vectors is necessary if they are not to become vanishingly small as we move up through the stratosphere. This problem was discussed, for example, by Edmon *et al.* (1980) and Palmer (1981). In practice it is found that multiplication of $\tilde{\mathbf{F}}$ by p^{-1} keeps magnitudes roughly comparable throughout the middle atmosphere. However, there appears to be no decisive theoretical justification for such a scaling[3] and we have instead adopted the simple expedient of plotting only the *direction* of $\tilde{\mathbf{F}}$ at each grid point in the meridional plane, with no attempt to draw arrows of the correct magnitude. This seemingly arbitrary procedure can be defended on the grounds that, perhaps of more interest than $\tilde{\mathbf{F}}$ itself in (2.4) is the quantity

$$\mathbf{c} \equiv \tilde{\mathbf{F}}/A, \tag{3.1}$$

which has dimensions of velocity. By analogy of (2.4) with the wave-action equation for slowly-varying linear conservative waves,

$$\frac{\partial \tilde{A}}{\partial t} + \nabla \cdot (\mathbf{c}_g \tilde{A}) = 0 \tag{3.2}$$

(Bretherton and Garrett 1968), where $\tilde{A}$ is the wave-action density and $\mathbf{c}_g$ the group velocity, one can choose to regard $\mathbf{c}$ as a "velocity of wave-activity propagation", or an extension of the concept of group velocity to cases where the approximation of slowly-varying wave fails. However, since A is not calculable accurately in the present model, we are unable to determine the magnitude of $\mathbf{c}$; all we can say is that its direction is parallel, or antiparallel, to that of $\tilde{\mathbf{F}}$, depending on the sign of A (see Section 2). Thus our arbitrarily normalized $\tilde{\mathbf{F}}$ vectors give us some feel for the ray paths, along which wave-activity propagates.

We must now discuss our plotting of the contours of $\nabla \cdot \mathbf{F}$. In this case the p-coordinate version (2.3) is much more convenient than the z-coordinate form, which is proportional to p times (2.3) [see Eq. (A3)]. The reason is that (2.3) only varies by an order of magnitude or so throughout the middle atmosphere, while the z-coordinate form varies by many orders of magnitude. Moreover, there is now good justification for plotting (2.3) as it stands, irrespective of the vertical coordinate, since it is this form (divided by $a\cos\phi$, but with no factor p^{-1}) which appears in the transformed momentum equation (2.7) [contrast Dunkerton *et al.*, 1981, Eq. (A2a)]. Of course the use of (2.3) and the arbitrary scaling of $\tilde{\mathbf{F}}$ means that the apparent convergence or divergence of the arrows need bear no relation to the plotted contours of $\nabla \cdot \mathbf{F}$.

4. GCM description and basic behavior

Before we can discuss the model results and their interpretation, it is important that the design and performance of the GCM be well established. Otherwise, it would be very difficult to evaluate the significance of the model E-P flux diagnostics described above.

The 40-level "SKYHI" GCM used in this study is a higher resolution and somewhat modified version of that described by FMSS. The horizontal grid is latitude–longitude with energy-conserving second-order finite differencing and Fourier filtering at higher latitudes. In the vertical grid, a modified "sigma" coordinate system is utilized which becomes an isobaric system above ~350 mb (for details, see FMSS). The vertical

[3] M. E. McIntyre (personal communication, 1982) has suggested that planetary wave "breaking" (see McIntyre, 1982) could provide a rationalization of this empirical result.

grid spacing can be seen in the tic marks on the right hand ordinates in Figs. 1–3.

The only parameterization for this model not described in FMSS or its predecessors is that of vertical subgrid-scale diffusion. The approach used here is a "dry" version of the moist Richardson-number-dependent heat and momentum diffusivities described by Levy *et al.* (1982, Appendix A).

The most significant modification of the GCM since the FMSS study is the incorporation of an increase in the horizontal grid resolution. The FMSS version used a 9° latitude by 10° longitude grid, while the present study uses a 5° latitude by 6° longitude grid.

Another important modification of the model since the FMSS experiment is that the effective magnitudes of the horizontal subgrid-scale diffusion coefficients have been decreased by a factor of 3 beyond that already implied by the switch to higher horizontal resolution. This has been accomplished by changing the traditional Smagorinsky (1963) nonlinear diffusion coefficient,

$$K_H = k_0^2(\Delta y)^2|D|, \tag{4.1}$$

to

$$K_H^* = \frac{1}{3} k_0^2(\Delta y)^2|D|^* \tag{4.2}$$

Here, K_H is the horizontal diffusion coefficient, $k_0 = 0.2$, Δy the meridional grid spacing and $|D|$ the horizontal velocity deformation. The modified version $|D|^*$ is similar to $|D|$, except that its finite differencing is constructed so as to be more sensitive to single grid interval wind velocity variations. The net effect of these two changes is to increase significantly the scale selectivity of the model horizontal diffusion. Details of this scheme will be described in a later paper.

The use of this reduced magnitude of diffusivity arose from a series of observations of the strengths and weaknesses of various GCMs. In particular, it has been found that some spectral transform models give significantly worse results at higher horizontal resolution than obtained from equivalent finite-difference models. This was surprising in view of the generally acknowledged superiority of spectral transform model simulations over those of grid-point models at lower horizontal resolutions. These results led us to hypothesize that many spectral models (particularly those using biharmonic horizontal diffusion and no vertical diffusion) have been unrealistically *underdissipative* at higher resolutions. The counterpart hypothesis is that many finite-difference models (particularly those using "Smagorinsky" horizontal diffusion) have been unrealistically *overdissipative* at lower horizontal resolutions. To examine this latter hypothesis, we modified the GCM to include Eq. (4.2) as the model horizontal subgrid-scale diffusion coefficient. Tests of this modification have shown that over half of the simulation improvements achieved here relative to FMSS have been attributable to the decreased horizontal diffusion, while the remaining improvement is related to the improved horizontal resolution.

As in FMSS, annual mean insolation is used. At this stage in our research, we find that elimination of the annual cycle allows simpler insights for a number of physical questions. We recognize, however, that this simplification may lead to model phenomena which are unrepresentative of the actual atmosphere. Complete simulations, of course, require that the annual cycle of insolation be included. For an example of an annual cycle simulation with the lower resolution version of this model, see Mahlman and Sinclair (1980). The increase in horizontal resolution was implemented by interpolation from the lower resolution version on day 500 (time after spinup from rest on day zero). The lowered horizontal diffusion was added on day 844. The analysis presented here is for the period from day 1229 to 1259, with sampling being taken six times per model day. This relatively high sampling frequency was found to be necessary to reduce aliasing of the analysis results due to higher frequency model gravity waves. Logistically, these sampling choices made it necessary to process 60 model data tapes. This constraint precluded use of a sampling period longer than 30 days.

The two major changes to the model have led to some new results relative to those presented in FMSS. Fig. 1 shows a meridional cross section of the zonal wind (u) averaged over all longitudes and over the 30-day period. A comparison of Fig. 1 with Fig. 5.3a in FMSS shows some important differences. In the troposphere, the westerly jets are stronger, more clearly defined and lie slightly poleward of those in FMSS. In this simulation, the equatorial upper tropospheric westerlies are weaker (maximum $\bar{u}$ is now 9 m s^{-1} compared to 15 m s^{-1} previously). The surface westerlies now lie closer to their proper positions in midlatitudes. In each case, these results correspond to a lessening (but not disappearance) of a previous model defect.

For the middle atmosphere, comparison of Fig. 1 with Fig. 5.3 in FMSS shows a remarkable difference. In the mesosphere, the midlatitude westerly jets are now "closed off" with maxima near 65 km. Previously, the jets showed their strongest intensities at the highest model level. This is a point of some significance, because of the very strong current interest in the dynamical cause of the closed-off jet in the middle mesosphere (e.g., Lindzen, 1981; Holton, 1982; Matsuno, 1982). Over most of the stratosphere, however, the midlatitude westerlies are somewhat stronger than in the previous model. Consistent with this, the zonal mean temperature ($\bar{T}$) field in Fig. 2 shows a somewhat decreased magnitude of the reversed meridional gradient in the lower stratosphere in comparison to the $\bar{T}$ field shown in Fig. 3.1b in FMSS. In the mesosphere, however, the $\bar{T}$ field in Fig. 2 now shows a reversed

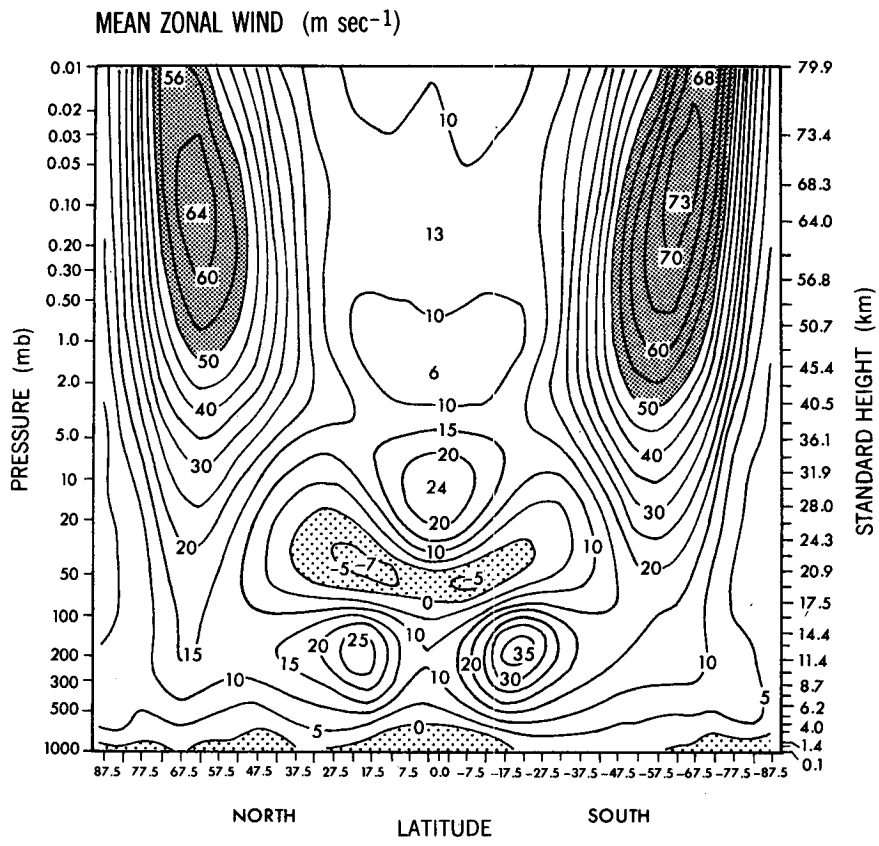

FIG. 1. Zonally averaged zonal wind $\bar{u}$ (m s^{-1}). The period of averaging is 30 days with sampling taken six times per model day.

meridional gradient with higher latitudes being as much as 8–15°C warmer than equatorial latitudes. In FMSS the higher latitudes were about 6°C colder than equatorial regions.

In lower latitudes the most remarkable difference shown by Fig. 1 is the now clear presence of an isolated westerly jet centered at the equator between about 25–35 km with a maximum speed of 24 m s^{-1}. In the previous model, the equatorial westerly jet was less isolated from the midlatitude jets, and was located at about 35–45 km with a maximum speed of 37 m s^{-1}. In the present model, there is a minimum westerly speed of 6 m s^{-1} at ~45 km and a weak westerly maximum of 13 m s^{-1} near 60 km. Previously, the model 60–80 km region was occupied by weak easterlies.

In many ways these simulation differences are dramatically large, considering that the only significant changes are improved horizontal resolution and decreased horizontal viscosity. In fact, the zonal wind differences are larger than those previously found in FMSS by reducing the ozone amount by 50%. For these large differences, it is of interest to be able to explain why they occur.

5. Diagnostic analysis

a. Wave-propagation diagnostics

In Fig. 3 we present a meridional cross section of $\tilde{\mathbf{F}}$-arrows, arbitrarily normalized at each point, and contours of $\nabla \cdot \mathbf{F}/a \cos\phi$. Each of these quantities has been averaged over the 30 day period described in Section 4. To facilitate interpretation, the values of $\nabla \cdot \mathbf{F}/a \cos\phi$ have been subjected to a 1–2–1 smoothing operator applied in the y and p directions.

The arrows give an indication of the "ray paths" of wave-activity propagation. In general, these rays extend upward and somewhat poleward out of the troposphere. As they penetrate higher, they tend to acquire an equatorward tilt; some of them (those nearer the equator) become almost horizontal as they proceed toward the tropics in the middle stratosphere, while others (further poleward) move up into the mesosphere. These arrow directions are very similar to the January observational values given by Hamilton (1982). Note, however, that the true F-vectors (as opposed to the arbitrarily normalized vectors shown here) are of much smaller magnitude in the mesosphere than in the stratosphere.

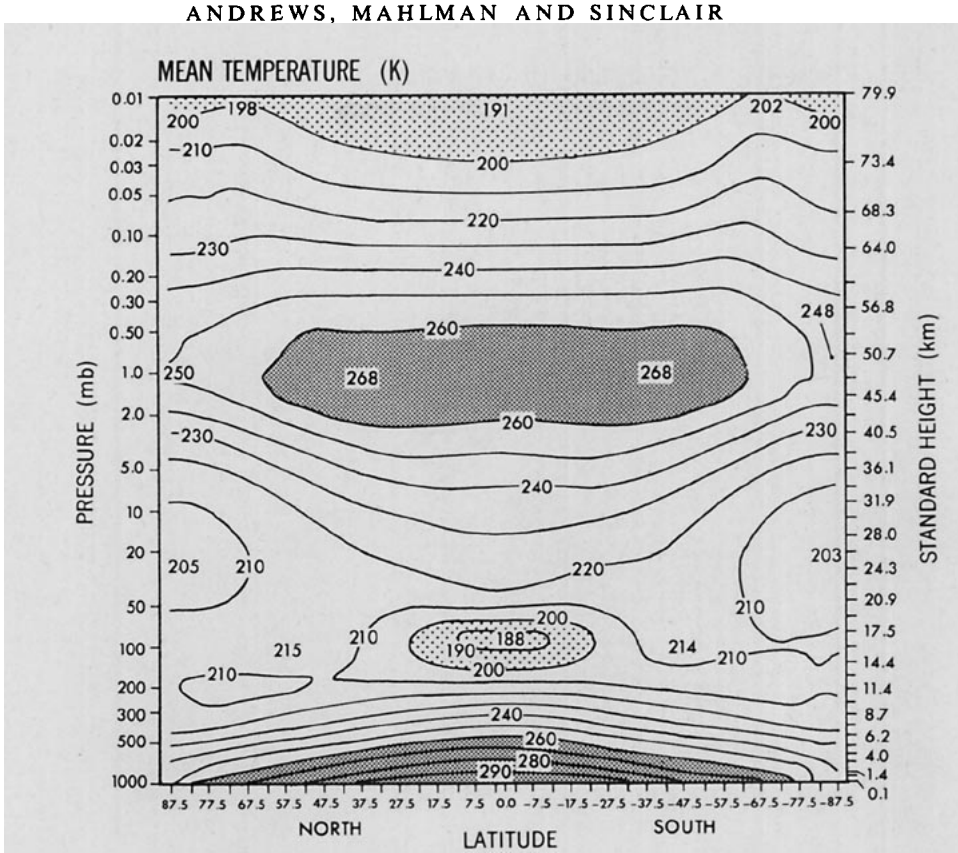

FIG. 2. Zonally averaged temperature (K) for the 30-day analysis period.

The equatorward penetration of rays has been shown by Karoly and Hoskins (1982) to be a typical feature of the behavior of planetary waves of small meridional scale on a spherical earth. The ray paths, however, are somewhat modified by zonal wind structure (Matsuno, 1970). Note, for example, that Figs. 1 and 3 indicate a tendency for the ray paths to refract around the subtropical jets. On the other hand, we find that the upward arrows in the midlatitude mesosphere are associated with predominantly wavenumber 1 disturbances which are of large latitudinal scale and can propagate into the upper westerlies in both hemispheres.

It should be observed that the arrows follow complicated paths in the equatorial regions. This is consistent with the fact that the interpretation of the arrows is ambiguous there. As mentioned above, the ambiguity arises because some equatorial modes (notably Kelvin waves), unlike midlatitude planetary waves, have negative values of A. For such waves, the direction of wave-activity propagation, as measured by the velocity $\mathbf{c}$ defined in (3.1), is opposite to that of $\mathbf{F}$. Since we are unable to compute A in the model we cannot say precisely where it changes sign. However, it is likely to be negative, for instance, in the equatorial region between 17 and 25 km where downward-pointing arrows occur. Alternative "SKYHI" model analysis (Hayashi *et al.*, 1984) has shown that Kelvin waves predominate there.

From (2.4) it can be seen that $\nabla \cdot \mathbf{F}$ is nonzero in regions of wave transience, wave dissipation or forcing, or wave nonlinearity. Moreover, $\nabla \cdot \mathbf{F}/a\cos\phi$ is the "wave-forcing" term in the transformed mean momentum equation (2.7) and this quantity is contoured in Fig. 3. In this subsection we discuss the physical wave processes which may lead to nonzero values of $\nabla \cdot \mathbf{F}$, while in Section 5b we examine the effects of nonvanishing $\nabla \cdot \mathbf{F}$ on the mean zonal momentum balance. Note, however, that because our data are averaged over a 30-day interval, *linear* wave transience (described by the time average of $\partial A/\partial t$) is probably a negligible contributor to the time-averaged $\nabla \cdot \mathbf{F}$. By contrast, nonlinear transience (such as occurs in the growth and decay of a large cyclone or planetary wave), may be reversible or irreversible (McIntyre, 1982); in the irreversible case dissipation prevents fluid particles from returning to their initial positions and the effects of transience do not average out. Thus, at finite amplitude, the "transience" and "dissipation" contributions to the average $\nabla \cdot \mathbf{F}$ may be intimately related.

In Fig. 3 we see that $\nabla \cdot \mathbf{F}/a\cos\phi$ is basically positive in the midlatitude lower troposphere, but negative

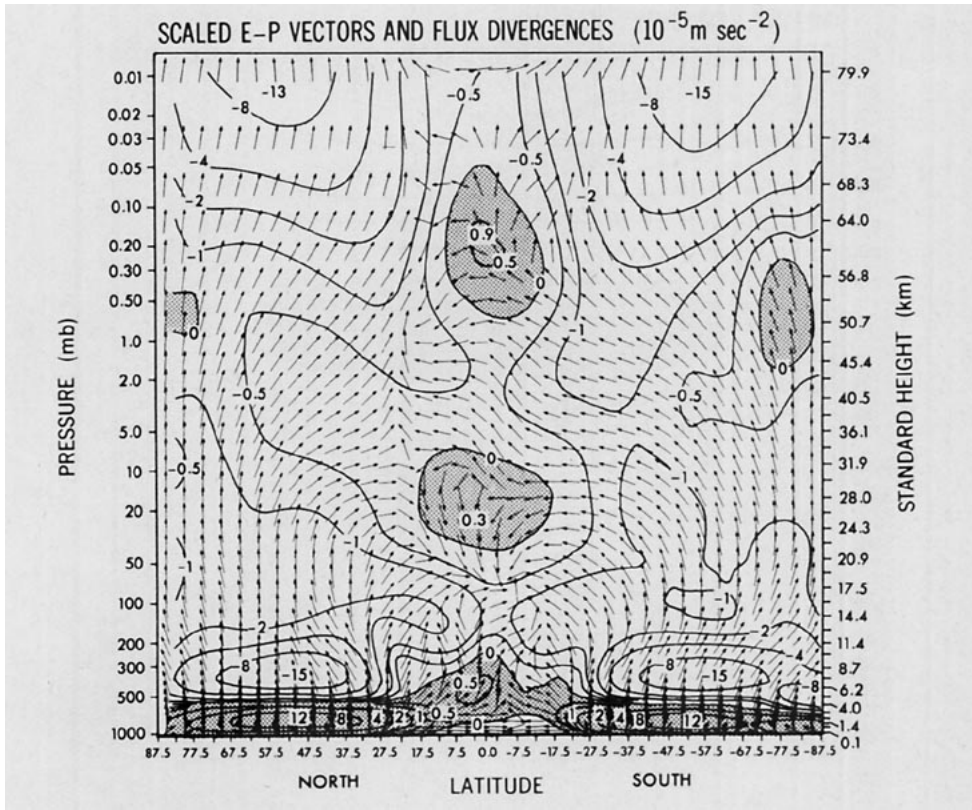

FIG. 3. Meridional cross section of Eliassen-Palm flux vector directions (arrows) and contours of Eliassen-Palm flux divergence normalized as zonal force per unit mass (10^{-5} m s^{-2}) for the 30-day analysis period. Vector magnitudes are not shown (see Section 3). Regions of positive Eliassen-Palm flux divergence (suggesting eddy produced acceleration of westerlies) are shaded.

throughout most of the midlatitude upper troposphere, stratosphere and mesosphere; largest negative values occur in the troposphere and upper mesosphere. In the tropics, regions of divergence are found near heights of about 28 and 60 km; these are predominantly due to Kelvin wave dissipation in the westerly jets (cf. Fig. 1) (Hayashi *et al.*, 1984). Such westerly wind regions are well-known to be regions where wave dissipation is likely to be enhanced (e.g., Holton, 1975, p. 142). The large negative values in the upper midlatitude mesosphere are mainly attributable to dissipation of model planetary waves. In the tropical upper mesosphere, gravity waves and planetary waves contribute about equally.

In the troposphere, the mechanisms of transience, dissipation or forcing and nonlinearity are all likely to be important. Note that the values of $\nabla \cdot \mathbf{F}/a \cos\phi$ are quite large in the midlatitude troposphere. The sign change at about 600 mb in midlatitudes is probably due to the presence of baroclinically unstable disturbances which grow and decay there. Support for this view comes from the idealized experiments on baroclinic wave life cycles described by Edmon *et al.* (1980), in which the time-averaged $\nabla \cdot \mathbf{F}$ shows just such a sign change (albeit at the lower level of about 800 mb).[4] Simple arguments, using Eqs. (B8) or (B12), with appropriate boundary conditions, verify that such a pattern of $\nabla \cdot \mathbf{F}$ tends to accelerate the weak low-level westerlies and decelerate the stronger westerlies in the upper troposphere. This tendency of the eddies to reduce the vertical wind shear in the troposphere is consistent with the tendency to reduce the pole-to-equator temperature gradient implied by the *net* increase of total poleward transport of heat that occurs in the presence of baroclinic waves. Note that this diagnostic interpretation is in sharp contrast to the implied "traditional" view (e.g., Lorenz, 1969) of the midlatitude westerlies being accelerated due to the observed presence of large eddy momentum flux convergences there.

The tropospheric magnitudes of $\nabla \cdot \mathbf{F}/a \cos\phi$ in Fig. 3 are similar to, but somewhat larger than, the observed quasi-geostrophic potential vorticity fluxes first cal-

[4] This sign change in the troposphere is also found at about 800 mb in the observational results in Wiin-Nielsen and Sela (1971) and Edmon *et al.* (1980).

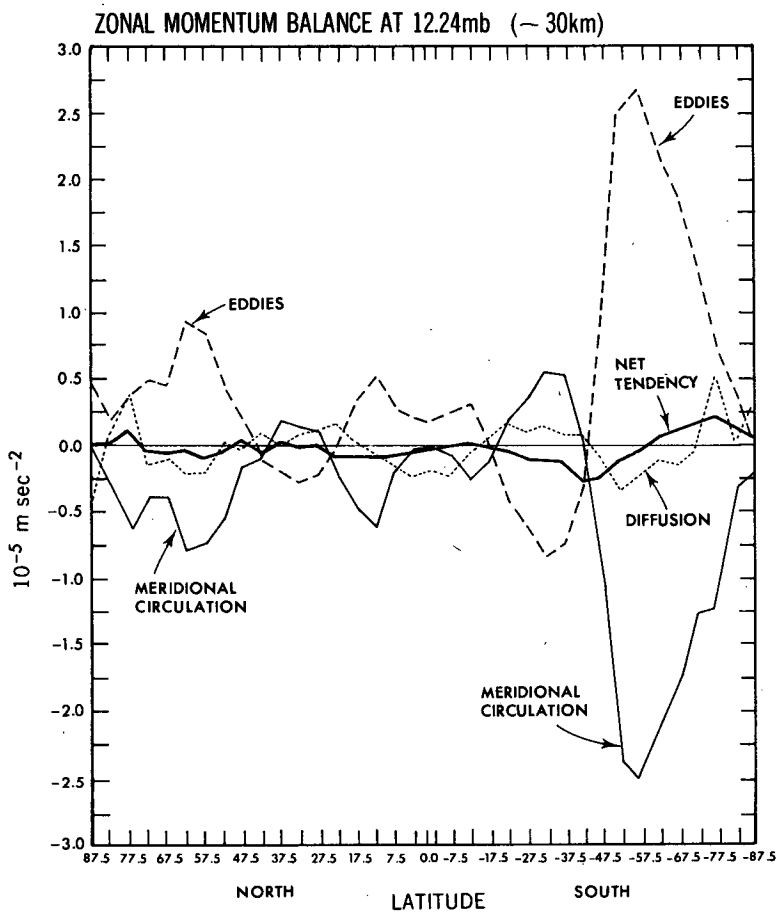

FIG. 4. Zonal momentum balances (10^{-5} m s^{-2}) at 12.24 mb for the 30-day analysis period using the familiar Eulerian-mean form of Eq. (2.5). "MERIDIONAL CIRCULATION" represents the terms in brackets in Eq. (2.5), while "EDDIES" represent the terms in braces in Eq. (2.5). "NET TENDENCY" is the time change of $\bar{u}$ and "DIFFUSION" represents the sum of model vertical and horizontal subgrid-scale diffusion terms.

culated by Wiin-Nielsen and Sela (1971). The equivalence between this flux and the quasi-geostrophic form of $\nabla \cdot \mathbf{F}/a \cos\phi$ suggests that the model processes described above are quite similar to those operative in the actual atmosphere.

b. Mean zonal momentum balance

We now examine the separate "mean flow" and "eddy" or "wave" contributions to the mean zonal acceleration as described both by the standard Eulerian-mean equation (2.5) and the transformed equation (2.7). For various levels we plot separate contributions to the momentum budget as functions of latitude, once again using 30-day means of (2.5) and (2.7) for our selected period.

Fig. 4 shows the standard separation at a pressure of 12.24 mb (~30 km), with the terms in brackets in (2.5) being referred to as the "MERIDIONAL CIRCULATION" and the terms in braces in (2.5) being called "EDDIES".[5] We see that throughout much of the latitudinal domain (and especially in the Southern Hemisphere) those two terms tend to oppose each other, while the frictional term $\bar{X}$ and the net tendency $\partial\bar{u}/\partial t$ are generally much smaller. Such an "eddy-meridional circulation" cancelation is often found in observed and simulated mean momentum balances (e.g., Vincent, 1968; Manabe and Hunt, 1968; Manabe and

[5] These zonal momentum balances are "exact" in the sense that the computational residuals at each latitude are effectively zero (to roundoff error of the computer). This is in sharp contrast to previous published GCM balances which generally had to rely upon an ambiguous transformation from "sigma" to p coordinates (Mahlman and Moxim, 1976).

Mahlman, 1976). The marked difference in the degree of cancelation between the two hemispheres is not a climatic feature of the model. Rather, it occurred due to a transient "burst" of planetary wave amplitude in Southern Hemisphere midlaltitudes during the last 10 days of the 30-day sampling period.

Figure 5 exhibits quite a different balance of terms in the time-averaged transformed mean momentum equation (2.7). The "RESIDUAL CIRCULATION" term [in the brackets in (2.7)] and the E-P flux divergence (EPFD) term (in the braces) still tend to compensate each other, although not to as great a degree as in the Southern Hemisphere event in Fig. 4. (Some remarks on the reasons for the cancelation between eddy and mean-flow terms in both formalisms are made in Appendix B.) Note that the E-P flux divergence in Fig. 5 is similar in both hemispheres in spite of the much larger Southern Hemisphere cancelation shown in Fig. 4.

An important observation to be made from comparing Figs. 4 and 5 is that, in middle and higher latitudes, the interpretation of the relative roles of eddy and mean-flow terms is *opposite* in the two momentum balance formalisms; for example, while the eddy contributions at these latitudes appear to be acting to accelerate westerlies in Fig. 4, they appear to be acting to decelerate westerlies in Fig. 5.

In the tropics, on the other hand, the two approaches give very similar results. The 12.24 mb level shown in Figs. 4 and 5 corresponds to the center of the equatorial westerly jet shown in Fig. 1. In each case the existence of the westerly jet is "explained" by an eddy momentum flux convergence. The analysis of Hayashi *et al.* (1984) indicates that this momentum flux convergence is attributable to dissipation of eastward moving Kelvin waves in the vicinity of this level. The dominance of Kelvin waves helps to explain the similarity beween the two approaches in the tropics. For

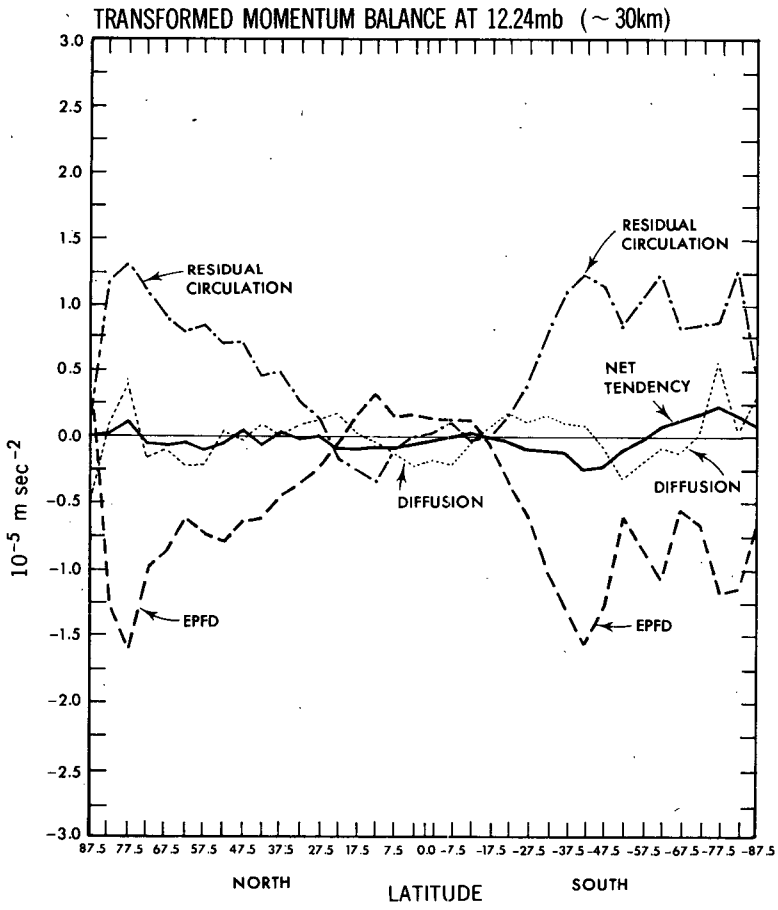

FIG. 5. Transformed zonal momentum balances (10^{-5} m s^{-2}) at 12.24 mb for the 30-day analysis period. "RESIDUAL CIRCULATION" represents the terms in the brackets in the transformed Eq. (2.7), while "EPFD" is the Eliassen-Palm flux divergence term in the braces in Eq. (2.7). "NET TENDENCY" and "DIFFUSION" terms are the same as in Fig. 4.

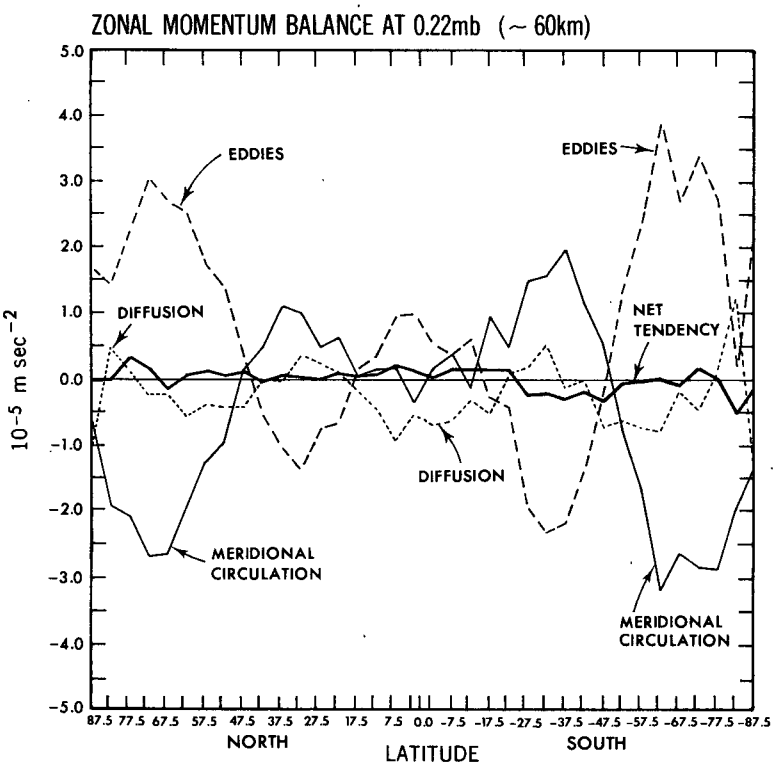

FIG. 6. As in Fig. 4, except at 0.22 mb.

pure Kelvin waves, $v' = 0$, so $\psi = 0$ by Eq. (2.2), and hence $(\bar{v}, \bar{\omega}) = (\bar{v}^*, \bar{\omega}^*)$ by Eq. (2.6). Because the model Kelvin waves do tend to have small v', the similarity between $(\bar{v}, \bar{\omega})$ and $(\bar{v}^*, \bar{\omega}^*)$ is to be expected.

Figures 6 and 7 show the respective contributions to the two mean momentum equations at 0.22 mb (~60 km). The "MERIDIONAL CIRCULATION" term in Fig. 6 clearly shows the contribution of the well-known "2-cell" indirect circulation with a comparatively large cancelation.

Note from Fig. 1 that 60 km is very near the peak of the westerly jets which are centered between 60–70°N and S. According to the traditional interpretation of the standard balances of Fig. 6 (e.g., Vincent, 1968; Manabe and Hunt, 1968), these westerly jets are "maintained" by eddy momentum flux convergence into them, thus balancing the deceleration due to the indirect "MERIDIONAL CIRCULATION" (essentially the Coriolis torque due to an equatorward $\bar{v}$). On the other hand, the transformed balances in Fig. 7 imply that the net effect of the midlatitude disturbances is to decelerate a zonal wind that would have been even stronger if no wave activity were present in the middle atmosphere.

Such a result is also in accord with Eqs. (B11) or (B12) which show in a simple quasi-geostrophic case how $\nabla \cdot \mathbf{F}$ can force departures from radiative equilibrium. Indeed, equations of this sort appear to come much closer to the most natural means of describing "the effect of the waves on the mean flow" in midlatitudes than other methods; for further discussion, see Appendix B.

Note again in Figs. 6 and 7 (as in Figs. 4 and 5) that the two formalisms give very similar results in the equatorial region. Both figures indicate significant westerly acceleration due to "eddies" irrespective of their interpretation. This corresponds to the area of E-P flux divergence seen in Fig. 3 near 60 km in the tropics. Fig. 1 shows that this is a region of a weak westerly maximum of 13 m s^{-1} (relative to levels above and below). The more detailed analysis of Hayashi *et al.* (1984) shows this to be a region of momentum deposition due to "fast" and "ultra fast" Kelvin waves (wavenumbers 1 and 2, eastward phase speeds ~80 and 120 m s^{-1}, respectively). Their spectral decomposition also indicates significant retardation of westerlies there due to shorter wavelength gravity waves. Thus, the net acceleration by waves in that vicinity indicated in Figs. 3, 6 and 7 is the result of competing accelerative mechanisms. The resemblance between the two formalisms in the equatorial regions of Figs. 6 and 7 can be explained by an extension of the arguments given above for Figs. 4 and 5. Here the equatorial eddy motion is dominated by Kelvin waves and

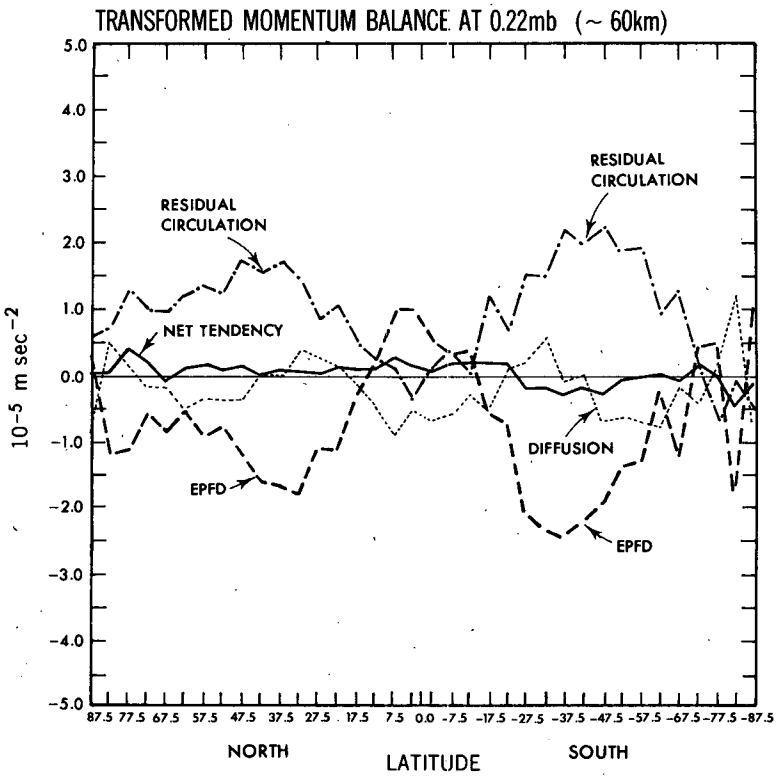

FIG. 7. As in Fig. 5, except at 0.22 mb.

smaller-scale gravity waves, neither of which is associated with significant values of $\overline{v'T'}$ or ψ.

Figures 6 and 7 also show that the "eddy"-induced westerly acceleration in the tropics is opposed mainly by westerly deceleration due to subgrid-scale diffusion. A more detailed analysis shows that most of this diffusive deceleration is due to vertical "low-Richardson-number" diffusion excited by the large model disturbance amplitudes in this region. This result may be compatible with the gravity wave analysis of Weinstock (1982) which indicates that induced diffusion is a necessary participant in the nonlinear evolution of gravity waves and their associated momentum deposition.

The momentum balances for the model upper mesosphere are presented in Figs. 8 and 9 for the 0.031 mb level (~73 km). The results for this pressure level should perhaps be accepted only with caution. This is the second model level from the top and previous numerical experiments have indicated that the second level is affected somewhat when this model's upper boundary condition is changed. Nevertheless, some interesting processes are occurring here which are worthy of note, particularly since this is the altitude above the "closed off" midlatitude westerly jets shown in Fig. 1.

Note in Figs. 8 and 9 that, except in polar latitudes, the "EDDIES" and the E-P flux divergence are generally of the same sign and look quite similar. However, the magnitude of the E-P flux divergence is now the larger, reaching as high as -7×10^{-5} m s^{-2}. The two components of $\nabla \cdot \mathbf{F}$ [see (2.3)] tend to take the same sign, rather than opposing each other (see Appendix B), indicating strong departures from nonacceleration conditions. We hypothesize that this results from the very large disturbance amplitudes and attendant mechanical dissipation present there. In fact, at this model level the "eddy mechanical dissipation time" (eddy kinetic energy divided by the dissipation of eddy kinetic energy) is about 0.6 days. An exception to this is near the pole where the eddy dissipation rates are much smaller, mostly because of the diminished model gravity wave amplitudes there. At polar latitudes, the eddy mechanical dissipation time is about 5 days, implying somewhat weaker departures from nonacceleration conditions.

Finally, we argue that it is the much larger values of E-P flux convergence in the mesosphere that are responsible for this model version's simulation of the closed off higher latitude westerly jets. In the lower resolution, higher horizontal diffusion model version reported in FMSS, most of the disturbances were dissipated before reaching the mesosphere. However, the lesser damping of disturbances in this model leads to stronger winds in the middle stratosphere (with as-

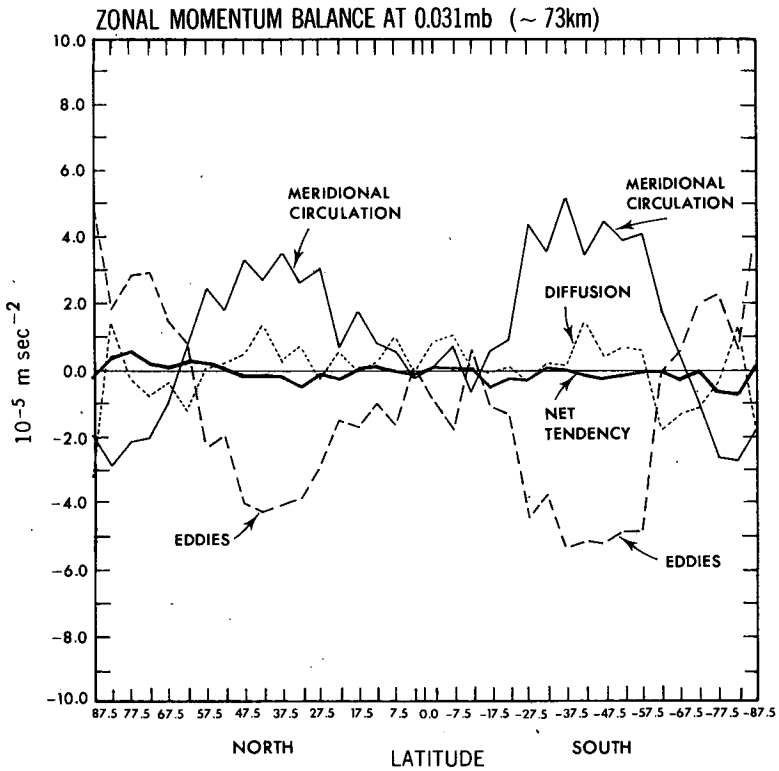

FIG. 8. As in Fig. 4, except at 0.031 mb.

sociated stronger meridional temperature gradients) than shown in FMSS.

Unfortunately, the above results do not really resolve the question of how much mechanical damping of large-scale disturbances is appropriate. The question is made vastly more complicated by the presence of gravity waves in the real atmosphere on scales below that resolved by this model. Such waves not only can transfer momentum on their own but might also interact nonlinearly to excite enhanced mechanical dissipation of disturbances at all spatial scales.

6. Effect of removing eddies in the middle atmosphere

The E-P diagnostics presented here suggest ways of interpreting eddy mean-flow interaction which can differ greatly from inferences based on "traditional" diagnostics. However, one may still be left with the question as to which interpretation is the more meaningful.

Here we attempt to resolve this question through use of a demonstration numerical experiment using the same "SKYHI" model. In this experiment, we introduce into the model a strong Newtonian/Rayleigh type damping of eddy quantities in the model lower stratosphere of the form

$$\text{DAMPING TERMS} = -\frac{T', u', v'}{\tau_{\text{damp}}}. \quad (6.1)$$

Here, τ_{damp} is the imposed damping timescale and is set to a value of 0.05 days over the ~50–180 mb layer with sharp tapering to longer damping times above and below. The experiment was begun on model day 1190 and has been run for 80 additional days.

Introduction of the damping has the effect of markedly reducing the eddy kinetic energy of the model atmosphere at and above the damping layer (by more than a factor of 8). This is an indirect confirmation of the customary expectation that the stratosphere is not a region of significant *in situ* generated eddy activity. More importantly for this paper, however, is the response of the various model zonal wind maxima to the damping of nonzonal disturbances propagating upward out of the troposphere.

In middle and high latitudes the response of the lower stratosphere eddy damping is to produce a significant increase of $\bar{u}$ with the strongest winds now at the highest model level. At the top model level, the zonal winds have increased locally by as much as 50 m s^{-1}, while the strongest winds in each hemisphere have increased by 25–30 m s^{-1}. At the 65 km jet cores the zonal winds are about 15–20 m s^{-1} greater than shown in Fig. 1. In the middle stratosphere (10 mb), the strongest winds have increased by 12–15 m s^{-1} over those in Fig. 1. These results show clearly that using $\nabla \cdot \mathbf{F}$ in Eq. (2.7) to infer zonal momentum forc-

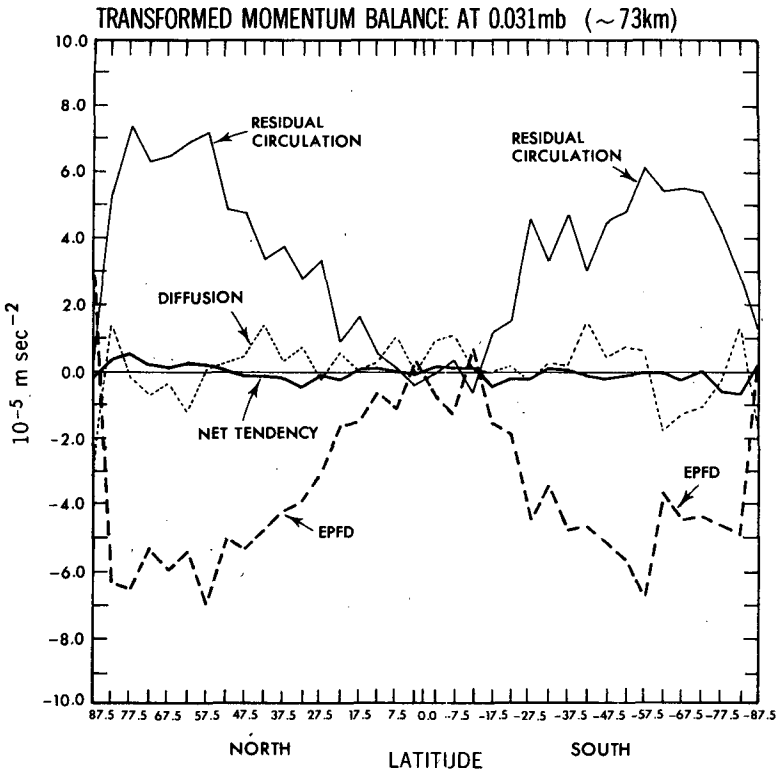

FIG. 9. As in Fig. 5, except at 0.031 mb.

ing is much more meaningful than using the traditional eddy momentum flux convergences of Eq. (2.5).

The tropical response to the eddy damping is less clear-cut. After 80 days the 10 mb equatorial westerly jet has decelerated by about 4 m s^{-1}. However, in this case, the deceleration appears as if it will continue for some time beyond the termination of the experiment. This is because in this experiment, the deceleration of the 10 mb westerly jet must occur mainly by radiative and diffusive damping. The decay of the jet due to radiative damping, however, is very slow since only extremely weak T gradients are required to keep an equatorial jet in thermal wind balance. This happens because the zonal kinetic energy of an equatorial jet is very large, relative to its zonal available potential energy; thus, radiative damping and subsequent thermal wind adjustment is expected to be very weak in equatorial jets compared to higher latitude jets. For this experiment then, it is not at all surprising that the midlatitude jets adjust rather quickly to a removal of eddies ($\nabla \cdot \mathbf{F} \rightarrow 0$) in comparison to the 10 mb equatorial jet (see also FMSS, Appendix C and Plumb and Bell, 1982).

In each case, the removal of eddies from the model middle atmosphere produces $\bar{u}$ accelerations compatible with the removal of the zonal wind forcing implied by $\nabla \cdot \mathbf{F}$. In extratropical latitudes, $\nabla \cdot \mathbf{F}$ is negative in the basic experiment; its removal leads to zonal westerly wind accelerations as expected from Eq. (2.7). For the tropical 10 mb jet, $\nabla \cdot \mathbf{F}$ is positive; its removal leads to rather slow deceleration of zonal westerlies.

7. Summary and conclusions

Several papers mentioned in the Introduction have suggested that Eliassen-Palm diagnostics may be valuable new tools for gaining insight into the dynamics of the atmosphere, as well as into the behavior of numerical models of particular atmospheric processes. Our experience with these diagnostics in the "SKYHI" GCM of the troposphere, stratosphere and mesosphere generally confirms this conclusion.

The E-P flux $\mathbf{F}$ has given a clear picture of planetary-wave propagation in the middle and high latitudes of the model, showing upward propagation from the troposphere and a tendency for equatorward and upward penetration in the stratosphere and mesosphere. However, the picture is more confusing in equatorial regions; additional diagnostics (e.g., those of Hayashi *et al.*, 1984) appear to be needed to clarify the description of wave propagation there.

We again find E-P diagnostics to be useful in the interpretation of the forcing of zonal-mean flows by eddies. They demonstrate that traditional interpreta-

tions ascribed to the various "eddy" and "meridional circulation" terms in the mean zonal momentum equation (2.5) do not provide a unique physical description of the processes involved. In fact, for most cases, the transformed momentum balance (2.7) provides a very different picture than does (2.5). For example, the transformed momentum balances in Figs. 5, 7 and 9 point to the important role of disturbances in decelerating extratropical westerly zonal flows from the upper troposphere to the upper mesosphere. This result is in distinct contrast to the traditional momentum balance approach which suggests an eddy-induced acceleration of midlatitude westerlies due to eddy momentum flux convergence (while neglecting the influence of the eddy heat flux on the mean flow). In the tropics, however, the two approaches give very similar results.

A test of which diagnostic approach is more meaningful has been made through a companion numerical experiment in which all eddy quantities are strongly damped in the lower stratosphere. This experiment shows that the zonal wind changes produced in response to removal of eddies are far better explained by the E-P diagnostics than by traditional momentum balances. This is not surprising in view of the fact that $\nabla \cdot \mathbf{F}$ (rather than the eddy momentum flux convergence) determines the forcing of the mean flow by the waves, as described for example by (B11) or (B13).

The E-P diagnostics also have provided us with useful indicators of the response to changes in model formulation, such as the changes of resolution and subgrid-scale diffusion, and has helped clarify the alteration in zonal wind structure produced by such changes.

It should be emphasized that we do not advocate the abandonment of the "traditional" Eulerian-mean diagnostic balances. We also caution against too naive an interpretation of the E-P flux and its divergence. For example, it should be remembered that $\nabla \cdot \mathbf{F}/a\cos\phi$ represents a *force* per unit mass due to the waves, and is not generally equal to the mean acceleration that is induced by this force. To calculate the latter, it is necessary to eliminate the residual mean meridional circulation and solve an elliptic equation [see Appendix B, especially Eq. (B8)]. Overall, in this work, we have found that a combination of the "traditional" and the E-P diagnostic approaches provides greater insights than either would if used in isolation.

It is well-known that zonal averaging is often quite inappropriate for studies of regional phenomena. Even for processes of global scale, any attempt to force atmospheric data into a zonally-averaged formulation, whether Eulerian or transformed-Eulerian, may well be unsatisfactory, particularly at higher latitudes. However, until even more physically-based diagnostics become available, the preliminary results described here suggest that E-P diagnostics, used with suitable caution, will provide valuable insights into the dynamics of general circulation models of the middle atmosphere.

Finally, we note that the GCM experiment described herein is for annual-mean insolation conditions. Such an idealization makes it much easier to interpret the phenomena featured in this work. This is because of the substantial complication added when time-dependent insolation is included. The complicating effects of the annual cycle are currently under study using a seasonal-cycle version of the GCM employed in this research.

Acknowledgments. We are indebted to Drs. S. B. Fels, Y. Hayashi, I. M. Held, C.-P. F. Hsu, M. E. McIntyre, R. A. Plumb and M. L. Salby and to the reviewers for their valuable comments on this research. Thanks are also due to L. Umscheid for his "SKYHI" model support, to J. Kennedy for her consistently high quality manuscript assistance and to the GFDL computer facility for their patience in handling the many tasks required for this work.

Support for D. G. Andrews was provided from NOAA Grant 04-7-022-44017 and at Oxford from a Royal Society Meteorological Office Research Fellowship.

APPENDIX A

Log-Pressure Form for the E-P Flux and its Divergence, and Computation of Diagnostics

The log-pressure coordinate form of the E-P flux (e.g., Dunkerton *et al.* (1981), Appendix A) can be shown to be related to our pressure coordinate form by

$$\tilde{F}_{(\phi)} = \frac{p}{p_0} F_{(\phi)}, \quad \tilde{F}_{(z)} = -\frac{1}{p_0} F_{(p)}, \tag{A1}$$

where

$$\left.\begin{aligned} z &= -\ln(p/p_0), \quad p = p_0 e^{-z} \\ p_0 &= 1013.25 \text{ mb.} \end{aligned}\right\} . \tag{A2}$$

The divergence of $\tilde{\mathbf{F}}$ in z-coordinates is

$$\nabla_{(z)} \cdot \tilde{\mathbf{F}} \equiv \frac{\partial(\tilde{F}_{(\phi)} \cos\phi)}{a\cos\phi\partial\phi} + \frac{\partial \tilde{F}_{(z)}}{\partial z}$$

$$= \frac{p}{p_0} \nabla \cdot \mathbf{F} = e^{-z} \nabla \cdot \mathbf{F}, \tag{A3}$$

using (A2) and (2.3). (Note that our notation differs from that of Dunkerton *et al.* in several respects. Most importantly, we use ∇ and $\mathbf{F}$ to denote p-coordinate quantities, while they use the same symbols for the z-coordinate versions.)

To represent the vector $\tilde{\mathbf{F}}$ in a rectangular plot with ϕ and z as coordinates, $\tilde{\mathbf{F}}_{(\phi)}$ and $\tilde{\mathbf{F}}_{(z)}$ are separately stretched in an obvious way. As mentioned in Section 3, the resulting $\tilde{\mathbf{F}}$ vectors decay rapidly with height;

we therefore multiply them by scalar normalizing factors, which differ from one grid point to another. These factors are chosen so that the resulting arrows are neither too long nor too short for clarity. They are, of course, everywhere parallel to the true scaled $\mathbf{F}$-vectors.

We note finally that care has been taken to ensure that the finite-difference (FD) approximations to $\nabla \cdot \mathbf{F}$ and the residual circulation, as calculated by the model, are of such a form that the FD version of the transformed zonal momentum equation (2.7) follows "exactly" (i.e., to within round-off error) from the FD version of the standard momentum equation (2.5). This means that we are assured of an exact balance of terms in the FD version of (2.7) at each latitude. Although, for example, the FD approximation to $(a\cos\phi)^{-1}(\partial F_{(\phi)}/\partial p)$ is not of standard second-order difference form, but deviates from it by an amount that is formally quadratic in the pressure increment between model levels.

APPENDIX B

Compensation between Mean Circulation and Eddies

In order to interpret the midlatitude momentum balances given in Section 5b, we consider a simplified system, namely quasi-geostrophic flow on a beta-plane. The Eulerian mean momentum equation (2.5) then reduces to

$$\bar{u}_t = [f_0\bar{v}] + \{-(\overline{u'v'})_y\} + \bar{X}, \tag{B1}$$

and the transformed equation (2.7) to

$$\bar{u}_t = [f_0\bar{v}^*] + \{\nabla \cdot \mathbf{F}\} + \bar{X}. \tag{B2}$$

Here y is northward distance, f_0 is a mean value of $f(y)$, and

$$\bar{v}^* = \bar{v} - (\overline{v'\theta'/\theta_p})_p, \tag{B3}$$

$$\nabla \cdot \mathbf{F} = -(\overline{u'v'})_y + (f_0\overline{v'\theta'/\theta_p})_p, \tag{B4}$$

in the present approximation. Unbracketed suffixes t, p and y denote partial derivatives. The corresponding transformed thermodynamic equation is

$$\bar{\theta}_t + \bar{\theta}_p\bar{\omega}^* = \bar{Q}, \tag{B5}$$

where $\bar{Q}$ is the Eulerian-mean diabatic heating, $\bar{\omega}^* = \bar{\omega} + (\overline{v'\theta'/\theta_p})_p$, and $\bar{\theta}_p = \bar{\theta}_p(p)$ under the quasi-geostrophic approximation.

Using the transformed continuity equation

$$\bar{v}_y^* + \bar{\omega}_p^* = 0, \tag{B6}$$

and assuming thermal wind balance

$$f_0\bar{u}_p = \frac{R}{p}\left(\frac{p}{p_0}\right)^{\kappa}\bar{\theta}_y = \frac{R}{p}\bar{T}_y \tag{B7}$$

(where R is the gas constant and p_0 is constant), we can eliminate $\bar{v}^*$ from (B2) and $\bar{\omega}^*$ from (B5) to obtain

$$\left\{\frac{\partial^2}{\partial y^2} + \frac{\partial}{\partial p}\epsilon\frac{\partial}{\partial p}\right\}\bar{u}_t = \frac{\partial^2}{\partial y^2}(\nabla \cdot \mathbf{F} + \bar{X}) - f_0(\bar{Q}_y/\bar{\theta}_p)_p, \tag{B8}$$

where

$$\epsilon(p) \equiv f_0^2\sigma^{-1} \quad \text{and} \quad \sigma(p) \equiv Rp^{-1}[\kappa\bar{T}p^{-1} - \partial\bar{T}/\partial p].$$

We can alternatively eliminate $\bar{u}_t$ and $\bar{\theta}_t$ to obtain

$$\left\{\frac{\partial^2}{\partial y^2} + \frac{\partial}{\partial p}\epsilon\frac{\partial}{\partial p}\right\}f_0\bar{v}^* = -\frac{\partial}{\partial p}\epsilon\frac{\partial}{\partial p}(\nabla \cdot \mathbf{F} + \bar{X}) - f_0(\bar{Q}_y/\bar{\theta}_p)_p. \tag{B9}$$

(Of course, appropriate boundary conditions must generally be applied if these are to be solved for $\bar{u}_t$ and $\bar{v}^*$; for the stratosphere and mesosphere, however, $\bar{u}_t = \bar{v}^* = 0$ on all boundaries should be fairly satisfactory in many cases.)

We first suppose that the waves are steady, conservative and linear, so that $\nabla \cdot \mathbf{F} = 0$ by the quasi-geostrophic version of (2.4), and that $\bar{X} = \bar{Q} = 0$. Then if $\bar{u}_t = 0$ on all vertical and horizontal boundaries and $\sigma > 0$, we have $\bar{u}_t \equiv 0$ everywhere: this is a special case of the "nonacceleration theorem" (Andrews and McIntyre, 1976, Boyd, 1976). Even under such "nonacceleration conditions," it is possible to have $(\overline{u'v'})_y \neq 0$, so that (B1) becomes

$$0 = \bar{u}_t = f_0\bar{v} - (\overline{u'v'})_y,$$

thus exhibiting perfect "compensation" or cancelation between nonzero Eulerian-mean circulation and eddy terms. However, in this case, (B2) reduces to

$$0 = f_0\bar{v}^*,$$

so that each of the terms on the right of (B2) vanishes individually.

This "nonacceleration" case, while a useful limit in some circumstances, is not an appropriate idealization of the model behavior described in Section 5b for at least two reasons. First, $\nabla \cdot \mathbf{F}$ is not found to be negligible, in the sense of being a small residual in (B4). [But note that in the model stratosphere and lower mesosphere the terms $-(\overline{u'v'})_y$ and $(f_0\overline{v'\theta'/\theta_p})_p$ on the right of (B4) do tend to take opposite signs, as can be seen from Figs. 4–7. On the other hand, in the upper mesosphere, they tend to take the same sign.] Eqs. (B8) and (B9) show that $\nabla \cdot \mathbf{F}$ influences both $\bar{u}_t$ and $f_0\bar{v}^*$; the relative sizes of the responses in $\bar{u}_t$ and $f_0\bar{v}^*$ depend on the horizontal and vertical scales of $\nabla \cdot \mathbf{F}$ (I. M. Held, personal communication, 1982). If $\bar{X} = \bar{Q} = 0$, then qualitative resemblance between $\bar{u}_t$ and $\nabla \cdot \mathbf{F}$ may be expected (see Dunkerton *et al.*, 1981).

A second reason for the irrelevance of the "nonacceleration limit" to the present work is the fact that 30-day time averages have been taken. The reason is

that when averages are performed over 30 days, the mean diabatic term $\bar{Q}$ enters the time-averaged dynamics in a significant way. This can be shown by assuming for simplicity that $\bar{Q}$ is represented by

$$\bar{Q} = -(\bar{\theta} - \theta_r)/\tau_r, \tag{B10}$$

where $\theta_r(y, p)$ is a radiative equilibrium potential temperature profile and $\tau_r(p)$ is a relaxation time. It is convenient to introduce a zonal wind u_r, defined to be in thermal wind balance with θ_r; then substitution of (B10) into (B8) and use of (B7) and its counterpart relating $\partial u_r/\partial p$ and $\partial\theta_r/\partial y$ gives

$$\left\{\frac{\partial^2}{\partial y^2} + \frac{\partial}{\partial p}\epsilon\frac{\partial}{\partial p}\right\}\bar{u}_t + \frac{\partial}{\partial p}\frac{\epsilon}{\tau_r}\frac{\partial}{\partial p}(\bar{u} - u_r) = (\nabla\cdot\mathbf{F} + \bar{X})_{yy}. \tag{B11}$$

Defining a time average

$$\langle\cdots\cdots\rangle = \frac{1}{\tau_a}\int_t^{t+\tau_a}(\cdots\cdots)dt,$$

we now find

$$\left\{\frac{\partial^2}{\partial y^2} + \frac{\partial}{\partial p}\epsilon\frac{\partial}{\partial p}\right\}\frac{\bar{u}(t+\tau_a) - \bar{u}(t)}{\tau_a} + \frac{\partial}{\partial p}\frac{\epsilon}{\tau_r}\frac{\partial}{\partial p} \times \langle\bar{u} - u_r\rangle = \langle\nabla\cdot\mathbf{F} + \bar{X}\rangle_{yy}. \tag{B12}$$

Providing that changes in $\bar{u}$ over the averaging period are not much greater than $\langle\bar{u} - u_r\rangle$ and that $\partial^2/\partial y^2 \leqslant \partial/\partial p(\epsilon\partial/\partial p)$ here, the relaxation term in $\langle\bar{u} - u_r\rangle$ will be significant if $\tau_a \gtrsim \tau_r$. For long time-averages ($\tau_a \gg \tau_r$), or relatively steady conditions, the balance will be

$$\frac{\partial}{\partial p}\frac{\epsilon}{\tau_r}\frac{\partial}{\partial p}\langle\bar{u} - u_r\rangle = \langle\nabla\cdot\mathbf{F} + \bar{X}\rangle_{yy}, \tag{B13}$$

or equivalently, $f_0^{-1}\langle\nabla\cdot\mathbf{F} + \bar{X}\rangle_y = -\langle\bar{v}^*\rangle_y = \langle\bar{\omega}^*\rangle_p = \langle\bar{Q}/\theta_p\rangle_p$.[6] In our model calculation, τ_a has been taken as 30 days, to average out shorter-period oscillations. This is rather greater than typical radiative relaxation times in the model's middle atmosphere and (B13) should be a reasonable first approximation. In such a case, $\langle\bar{u}_t\rangle$ will be quite small in the time-mean of (B2), and provided $\bar{X}$ is small (cf Figs. 5, 7 and 9), we will have midlatitude compensation between $\langle f_0\bar{v}^*\rangle$ and $\langle\nabla\cdot\mathbf{F}\rangle$, as found in the model. In the stratosphere and lower mesosphere, where the two terms comprising $\langle\nabla\cdot\mathbf{F}\rangle$ have opposite signs, this implies a comparable compensation between $\langle f_0\bar{v}\rangle$ and $\langle-(\overline{u'v'})_y\rangle$ (or their primitive equation counterparts), as in Figs. 4 and 6. In the upper mesosphere, where the two parts of $\langle\nabla\cdot\mathbf{F}\rangle$ are additive, compensation is smaller in the Eulerian-mean balance of Fig. 8 than in the transformed balance of Fig. 9.

[6] We are grateful to S. B. Fels for suggesting this approach to interpretation of the impact of radiative forcing.

REFERENCES

Andrews, D. G., and M. E. McIntyre, 1976: Planetary waves in horizontal and vertical shear: The generalized Eliassen-Palm relation and the mean zonal acceleration. *J. Atmos. Sci.*, **33**, 2031–2048.

——, and ——, 1978a: Generalized Eliassen-Palm and Charney-Drazin theorems for waves on axisymmetric mean flows in compressible atmospheres. *J. Atmos. Sci.*, **35**, 175–185.

——, and ——, 1978b: On wave-action and its relatives. *J. Fluid Mech.*, **89**, 647–664.

Boyd, J. P., 1976: The noninteraction of waves with the zonally averaged flow on a spherical earth and the interrelationships of eddy fluxes of energy, heat and momentum. *J. Atmos. Sci.*, **33**, 2285–2291.

Bretherton, F. P., and C. J. R. Garrett, 1968: Wavetrains in inhomogeneous moving media. *Proc. Roy. Soc. London*, **A302**, 529–554.

Dunkerton, T. J., C.-P. F. Hsu and M. E. McIntyre, 1981: Some Eulerian and Lagrangian diagnostics for a model stratospheric warming. *J. Atmos. Sci.*, **38**, 819–843.

Edmon, H. J., Jr., B. J. Hoskins and M. E. McIntyre, 1980: Eliassen-Palm cross sections for the troposphere. *J. Atmos. Sci.*, **37**, 2600–2616. (See also Corrigendum, 1981: *J. Atmos. Sci.*, **38**, 1115.)

Eliassen, A., and E. Palm, 1961: On the transfer of energy in stationary mountain waves. *Geofys. Publ.*, **22**, No. 3, 1–23.

Fels, S. B., J. D. Mahlman, M. D. Schwarzkopf and R. W. Sinclair, 1980: Stratospheric sensitivity to perturbations in ozone and carbon dioxide: Radiative and dynamical response. *J. Atmos. Sci.*, **37**, 2265–2297.

Hamilton, K., 1982: Some features of the climatology of the Northern Hemisphere stratosphere revealed by NMC upper atmosphere analysis. *J. Atmos. Sci.*, **39**, 2737–2749.

Hayashi, Y., D. G. Golder and J. D. Mahlman, 1984: Stratospheric and mesospheric Kelvin waves simulated by the GFDL "SKYHI" general circulation model. Submitted to *J. Atmos. Sci.*

Holton, J. R., 1975: *The Dynamic Meteorology of the Stratosphere and Mesosphere. Meteor. Monogr.*, No. 37, Amer. Meteor. Soc., 218 pp.

——, 1982: The role of gravity wave induced drag and diffusion in the momentum budget of the mesosphere. *J. Atmos. Sci.*, **39**, 791–799.

Hsu, C.-P. F., 1981: A numerical study of the role of wave-wave interactions during sudden stratospheric warmings. *J. Atmos. Sci.*, **38**, 189–214.

Karoly, D. J., B. J. Hoskins, 1982: Three-dimensional propagation of planetary waves. *J. Meteor. Soc. Japan*, **60**, 109–123.

Levy, H., II, J. D. Mahlman and W. J. Moxim, 1982: Tropospheric N_2O variability. *J. Geophys. Res.*, **87**, 3061–3080.

Lindzen, R. S., 1981: Turbulence and stress owing to gravity wave and tidal breakdown. *J. Geophys. Res.*, **86**, 9707–9714.

Lorenz, E. N., 1969: The nature of the global circulation: A present view. *The Global Circulation of the Atmosphere*, G. A. Corby, Ed., Roy. Meteor. Soc., 3–23.

Mahlman, J. D., and W. J. Moxim, 1976: A method for calculating more accurate budget analyses of "sigma" coordinate model results. *Mon. Wea. Rev.*, **104**, 1102–1106.

——, and R. W. Sinclair, 1980: Recent results from the GFDL troposphere–stratosphere–mesosphere general circulation model. Collection of Extended Abstracts Presented at ICMUA Sessions and IUGG Symposium 18, XVII IUGG General Assembly, December 1979, Canberra, 11–18. [Available from S. Ruttenberg, Secretary General, IAMAP, NCAR, P.O. Box 3000, Boulder, CO]

Manabe, S., and B. G. Hunt, 1968: Experiments with a stratospheric general circulation model. I. Radiative and dynamic aspects. *Mon. Wea. Rev.*, **96,** 477–539.

——, and J. D. Mahlman, 1976: Simulation of seasonal and interhemispheric variations in the stratospheric circulation. *J. Atmos. Sci.*, **33,** 2185–2217.

Matsuno, T., 1970: Vertical propagation of stationary planetary waves in the winter Northern Hemisphere. *J. Atmos. Sci.*, **27,** 871–883.

——, 1982: A quasi-one-dimensional model of the middle atmosphere circulation interacting with internal gravity waves. *J. Meteor. Soc. Japan,* **60,** 215–226.

McIntyre, M. E., 1980: An introduction to the generalized Lagrangian-mean description of wave, mean-flow interaction. *Pure Appl. Geophys.*, **118,** 152–176.

——, 1982: How well do we understand the dynamics of stratospheric warmings? *J. Meteor. Soc. Japan,* **60,** 37–65.

O'Neill, A., and C. E. Youngblut, 1982: Stratospheric warmings using the transformed Eulerian-mean equations and the effect of the mean state on wave propagation. *J. Atmos. Sci.*, **39,** 1370–1386.

Palmer, T. N., 1981: Diagnostic study of a wavenumber 2 stratospheric sudden warming in the transformed Eulerian-mean formalism. *J. Atmos. Sci.*, **38,** 844–855.

Plumb, R. A., and R. C. Bell, 1982: A model of the quasi-biennial oscillation on an equatorial beta plane. *Quart. J. Roy. Meteor. Soc.*, **108,** 335–352.

Sato, Y., 1980: Observational estimates of Eliassen and Palm flux due to quasi-stationary planetary waves. *J. Meteor. Soc. Japan,* **58,** 430–435.

Smagorinsky, J., 1963: General circulation experiments with the primitive equations. I. The basic experiment. *Mon. Wea. Rev.*, **91,** 99–164.

Vincent, D. G., 1968: Mean meridional circulations in the Northern Hemisphere lower stratosphere during 1964 and 1965. *Quart. J. Roy. Meteor. Soc.*, **94,** 333–349.

Weinstock, J., 1982: Nonlinear theory of gravity waves: Momentum deposition, generalized Rayleigh friction, and diffusion. *J. Atmos. Sci.*, **39,** 1698–1710.

Wiin-Nielsen, A., and J. Sela, 1971: On the transport of quasi-geostrophic potential vorticity. *Mon. Wea. Rev.*, **99,** 477–459.